Journal of
Marine Science and Engineering

MDPI

Article

The Performance of Low-Pressure Seawater as a CO_2 Solvent in Underwater Air-Independent Propulsion Systems

Eun-Young Park * and Jungho Choi

Department of Naval Architecture and Offshore Engineering, Dong-A University, Busan 49315, Korea; tamuchoi@dau.ac.kr

* Correspondence: pyy0924@naver.com; Tel.: +82-51-200-7938

Received: 2 November 2019; Accepted: 2 January 2020; Published: 3 January 2020



Abstract: Air-independent propulsion systems have improved the performance and decreased the vulnerability of underwater weapon systems. Reforming systems, however, generates large amounts of water and CO_2. The recovery or separation of CO_2, a residual gas component generated in vessels, entails considerable cost and energy consumption. It is necessary to understand the characteristics of the interaction between CO_2 and seawater under the conditions experienced by underwater weapon systems to design and optimize a CO_2 treatment process for dissolving CO_2 in seawater. In this study, numerical analysis was conducted using the derived experimental concentration and MATLAB. The diffusion coefficient was derived as a function of temperature according to the CO_2 dissolution time. Experiments on CO_2 dissolution in seawater were conducted. The concentration of CO_2 according to the reaction pressure and experimental temperature was obtained. The diffusion coefficient between CO_2 and seawater was found to be 6.3×10^{-5} cm^2/s at 25 °C and 7.24×10^{-5} cm^2/s at 32 °C. CO_2 concentration could be estimated accurately under vessel operating conditions using the derived CO_2 diffusion coefficients. Optimal design of the residual gas treatment process will be possible using the derived seawater–CO_2 diffusion coefficients under the actual operating conditions experienced by underwater weapon systems.

Keywords: carbon dioxide; CO_2 dissolution; underwater weapon systems; diffusion; diffusion coefficient

1. Introduction

Existing submarines are equipped with diesel propulsion systems, in which the energy for submerged operation is stored in lead-acid batteries. The capacity of these batteries limits the underwater range. The batteries are charged by a diesel generator during snorkeling, during which the submarine is exposed to a higher risk of detection [1]. Basically, the submarine is propelled by an electric motor and so the objective of the air-independent propulsion system is to silently generate electric energy when under the water. Electric energy can be produced with a diesel generator engine when the submarine is on the water surface or with a fuel cell with a reformer when the submarine is in military operation under the water. The steam reformer generates H_2 as fuel for the fuel cell and CO_2 vapor as a byproduct. However, CO_2 vapor cannot be discharged under the water during military operation because undissolved CO_2 will explode when rising up, which will be detected by others [2–4]. The current technology used still requires considerable cost and high energy consumption to recover or separate CO_2 discharged from vessels. Thus, technological innovation is required.

The aim of this research was to understand how CO_2 generated from a reformer fully dissolves in seawater in a short time period. Regarding studies on dissolution rate, Cavenati et al. [5] studied the adsorption of methane, CO_2, and N_2 by zeolite 13X under various pressures (0–5 MPa) and temperatures

(298, 308, and 323 K). The CO_2 adsorption capacity of zeolite 13X was much higher than its adsorption capacity for other gases and the adsorption capacity increased with the pressure. Dash et al. [6] conducted research on the solubility of CO_2 according to the reaction temperature (303–328 K) and CO_2 partial pressure (0.2–1500 kPa) in an aqueous solution of 2-amino-2-methyl-1-propanol and piperazine. Increasing the concentration of 2-amino-2-methyl-1-propanol and adding piperazine affected the absorption capacity, where the CO_2 absorption capacity of the solvent increased under a high operation pressure and low operating temperature. Manic et al. [7] measured the solubility of CO_2 in seven ionic liquids in the 8–22 MPa pressure range and at temperatures of 313.2 and 323.2 K. They found that the solubility of CO_2 increased when the pressure increased and the temperature decreased.

With regard to dissolution velocity, Hirai et al. [8] measured the CO_2 dissolution velocity while the flow velocity, temperature, and pressure conditions were varied. It was found that the dissolution velocity increased when the temperature, pressure, and flow velocity increased. Dang and Rochelle [9] measured the solubility of CO_2 and its absorption rate in monoethanolamine (MEA)/piperazine/water at 40–60 °C. The absorption rate of MEA with 0.6–1.2 M piperazine added was 1.5–2.5-times higher than that when MEA was used alone. Faiz and Al-Marzouqi [10] developed a model for absorbing CO_2 from natural gas at high pressures of up to 5000 kPa. They showed that the CO_2 removal rate increased with pressure, whereas the CO_2 absorption rate increased when chemical solvents, such as MEA, were used.

To understand the dynamic characteristics of CO_2, Lawal et al. [11] investigated the effects of operating conditions in CO_2 capture facilities and performed dynamic modeling to solve possible issues proactively. With regard to the modelling, the analysis was conducted using equilibrium- and velocity-based approaches. The authors mentioned that the velocity-based model provided better predictions of the chemical absorption process than the equilibrium-based model with regard to understanding the dynamic behavior of the absorber and the failure of the stripper. Munusamy et al. [12] measured the volumes of CO_2, N_2, CH_4, and CO and conducted research on their dynamic adsorption characteristics. The equilibrium adsorption capacities of each composition in the powder and granules of MIL-101(Cr) were measured at 288, 303, and 313 K. The CO_2 and CH_4 absorption of MIL-101(Cr) increased with the adsorption temperature.

Breault and Huckaby [13] simulated adsorber performance using multiphase computational fluid dynamics (CFD) that included heat transfer. They investigated the behavior and performance of the riser adsorber for the solid circulation rate, gas flow rate, and heat removal. CO_2 adsorption increased with the solid flow and it decreased with the gas flow. Zhang et al. [14] performed CFD for CO_2 capture at a membrane using methyldiethaneolamine and 2-(1-piperazinyl)-ethylamine. They intensively studied the membrane gas absorption (MGA) method for CO_2 separation, developed a 2D mass transfer model, and examined the effect of membrane performance on adsorption performance. Giammanco et al. [15] investigated the dynamic characteristics of CO_2 gas for an optimal ionic liquid system. They suggested that a large amount of gas can be dissolved in imidazolium-based ionic liquids. Kim et al. [16] examined the fluid dynamics and CO_2 removal efficiency of amine absorbents on a pilot scale with structured packing using a gas–liquid multiphase Euler CFD model.

Many studies have been conducted that focus on CO_2 capture technologies from the perspective of power generation efficiency. Although research and development have been performed and continuous investments in such CO_2 capture technologies have been made, studies conducted under actual operating conditions of underwater weapon systems are insufficient and it remains difficult to conduct research on the development and application of technologies in underwater weapon systems to design and optimize CO_2 dissolution in seawater. Although processes with high-pressure and high-temperature absorbents exhibit high CO_2 recovery efficiencies, the absorbents are costly and the conditions are different from the actual operating conditions of underwater weapon systems. In this study, seawater was used as a solvent for CO_2 absorption. In addition, the actual operating conditions of underwater weapon systems were simulated by performing the absorption process under normal pressure instead of high pressure.

In this study, dissolution experiments were performed and dynamic characteristics were analyzed according to pressure and temperature. These experiments were carried out by applying dissolution technology using seawater as a solvent without an absorbent to improve the treatment of CO_2 after hydrocarbon reforming. The experiments were performed at equilibrium pressures of 2–5 bar and the results were compared to those of the MATLAB numerical analysis. In addition, the seawater–CO_2 diffusion coefficient was derived under experimental conditions.

The remainder of this paper is organized as follows: Section 2 presents the experimental setup and procedure used in the study, Section 3 explains the modeling equations used in this work as well as the sensitivity analysis, while Section 4 discusses the results of this study. Section 5 concludes this paper.

2. Experimental Setup and Procedure

2.1. Experimental Setup

CO_2 generated after hydrocarbon reformation was injected using an absorption and equilibrium system, which employed a batch-type reactor (Figure 1).

The flow rate of each gas was maintained at a constant level using a mass flow controller (Line Tech, Daejeon, Korea) (MFC) allowing for gas of the desired composition to be introduced into the buffer tank and the reactor. The buffer tank supplied gases of each composition to the reactor after maintaining it at a constant temperature and pressure. The volumes of the buffer tank and reactor were both 9 L. The temperature and pressure of the buffer tank were measured using a thermocouple (Sunil Instrument, Busan, Korea) (TT) and pressure transmitter (Wika, Germany) (PI, PT) with 99.5% accuracy. Thermocouples (TT) and pressure transmitter (PT) are used to measure pressure and temperature, which are variables used to calculate the gas phase moles of a reactor.

During the test, the temperature and pressure were measured respectively and the measured values were recorded in the data logger.

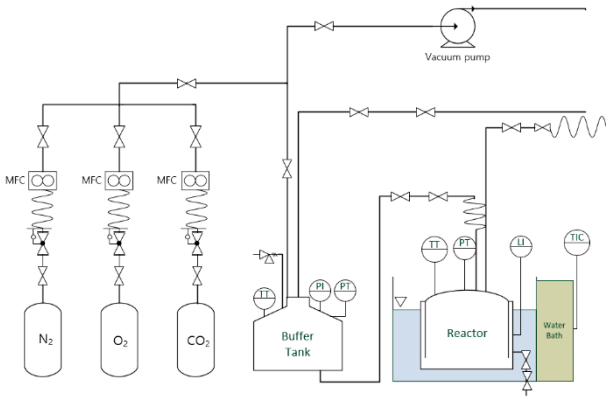


Figure 1. Schematic diagram of experimental apparatus.

2.2. Experimental Procedure

In the experiments, the impurities retained in the buffer tank, reactor, and piping were removed using a vacuum pump. After the reactor temperature was increased to the operating temperatures of 25 and 32 °C, 99.8% pure CO_2 was injected into the buffer tank until the operating pressure was reached. When the reactor pressure was stabilized to a constant level, the gas in the buffer tank was supplied to the reactor. The experimental conditions used to focus on the effects of solvent type, temperature, and pressure on CO_2 concentration are summarized in Table 1.

Table 1. Conditions of absorption experiments.

Gas Composition	Gas Concentration (%)	Absorbents	Temperature (°C)	Pressure (bar)
CO_2	More than 99.8	Distilled water Sea water	25, 32	2, 3, 5

All the solutions were tested in 99.9% pure distilled water (6 L) and seawater. For seawater, artificial seawater was fabricated and used in accordance with ASTM-D1141-98. Table 2 lists the composition of the artificial seawater [17].

Table 2. Chemical composition of synthetic seawater used in this study.

Compound	Concentration (g/L)
NaCl	24.53
$MgCl_2$	5.20
Na_2SO_4	4.09
$CaCl_2$	1.16
KCl	0.695
$NaHCO_3$	0.201
KBr	0.101
H_3BO_3	0.027
$SrCl_2$	0.025
NaF	0.003

At the initial stage, the buffer tank and reactor were isolated from each other and the empty buffer tank was pressurized with CO_2 and the reactor filled with solution in vacuum state. After, the pressure and temperature were stabilized in both chambers. The gas in the buffer tank was fed into the reactor via an isolation valve that, when open, resulted in a pressure decrease in buffer tank and increase in the reactor. The pressure and temperature were data logged until both tank pressures were stabilized, which was assumed to be equilibrium state.

2.3. Amount of Gas Dissolved as a Function of Pressure and Temperature

The CO_2 pressure was estimated from the pressure change in the system. To obtain the removal rate of the injected gas, the actual gas state equation was used. The number of moles of gas dissolved in the solvent in the reactor was calculated using the pressure and temperature of the buffer tank and those of the reactor, as shown in Equations (1) and (2) [18–20].

The initial number of moles of injected CO_2 (n_1) was calculated by substituting the pressure (P_1) and volume (V_1) of the buffer tank into Equation (1):

$$n_{CO_2} = \frac{PV}{zRT}, \tag{1}$$

where $z = V_{Actual}/V_{Ideal}$.

The compressibility factor (z) was adopted from HYSYS program, generally used in chemical process engineering, at a given pressure and temperature. The value varied from 0.975 to 0.99 in our research conditions.

The number of moles of CO_2 (n_2) at the equilibrium state between the buffer tank and the reactor could be calculated using the equilibrium pressure (P_2) and the sum of the volumes of the buffer tank and the reactor (V_2). The number of moles absorbed ($n_{CO_2,liq}$) was calculated as follows:

$$n_{CO_2,liq} = n_1 - n_2. \tag{2}$$

Here, pressure (P) is given in bar, temperature (T) is given in K, volume (V) is given in m^3, z is the compressibility factor and (n) is the number of moles of the gas. The gas constant (R) has the value $8.3144 \cdot 10^{-5}$ $\frac{bar \cdot m^3}{mol \cdot K}$.

3. Modelling Equations

Various models have been proposed for CO_2 absorption in amines, but few models use seawater or are implemented at normal pressure. The objective of this study was to develop a dynamic model of CO_2 absorption in seawater.

3.1. Governing Equation

A mathematical model of diffusion through a fluid was used to determine the amount of dissolution. The diffusion process is governed over time by the diffusion-advection equation. In this study, analysis was conducted in an unsteady state and the flow velocity of the fluid was ignored [21]. Fick's law of diffusion and binary aqueous diffusion coefficients were used for the mass transfer calculations. This was appropriate because the highest concentration of solutes occurred in the chamber liquid. At such concentrations, it is safe to assume that the CO_2 mainly interacts with water. Equation (3) is the resulting instationary conservation equation for each of the solutes:

$$\frac{\partial C}{\partial t} = D\Delta C, \tag{3}$$

where, C mol/m^3 is the concentration of the substance dissolved in the fluid and D m^2/s is the diffusion coefficient of the solute in the solvent, i.e., the material property of the substance.

3.2. Liquid-Phase Equation

The continuity equation for the unsteady state for CO_2 transport in the liquid phase of the reactor was obtained using Fick's diffusion law for the estimation of diffusion flux [22–27]:

$$N_A = k_g P(Y_A - Y_{Ai}) = k_l(C_{Ai} - C_A), \tag{4}$$

where:

1. N_A = molar flux of A, mol·cm^{-2}·s^{-1};
2. k_g = gas-phase mass transfer coefficient, (mol flue gas)·cm^{-2}·s^{-1}·atm^{-1};
3. k_l = liquid-phase mass transfer coefficient, cm·s^{-1};
4. Y_A = bulk gas-phase mole fraction of A, mol A/mol flue gas;
5. Y_{Ai} = interfacial gas-phase mole fraction of A, mol Ai/mol flue gas;
6. P = Total pressure, atm;
7. C_A = bulk liquid-phase concentration of A, mol A·cm^{-3};
8. C_{Ai} = interfacial liquid-phase concentration of A, mol Ai·cm^{-3}.

The gas-liquid equilibrium at the interface was calculated by the well-known Henry's law. Here, the Henry solubility constant is defined as H $= \frac{c_L}{p}$, where c_L is the concentration of a species in the aqueous phase and p is the partial pressure of that species in the gas phase under equilibrium conditions [28].

Henry's constant varies with the temperature of the system, as well as with the solvent and solute. Many researchers have derived Henry's CO_2 constants from 3.1×10^{-4} mol/m^{3}Pa to 3.6×10^{-4} mol/m^{3}Pa. A value of 3.4×10^{-4} mol/m^{3}Pa was used as Henry's constant in this model. The temperature dependence of the equilibrium constant can generally be explained by the Van't hoff equation, which also applies to the Henry law constant [28,29]:

$$H(T) = H^\circ \times exp\left[\frac{-\Delta_{sol}H}{R}\left(\frac{1}{T} - \frac{1}{T^\diamond}\right)\right], \tag{5}$$

where, H° at the reference temperature $T^\circ = 298.15K$, CO_2 $\frac{-\Delta_{sol}H}{R} = 2400$.

Using Equation (5), Henry's constant at 32 degrees Celsius for CO_2 was 2.79×10^{-4} mol/m^{3}Pa. The Henry's constant for seawater at 25 and 32 degrees Celsius was obtained as 3.01×10^{-4} mol/m^{3}Pa, 2.53×10^{-4} mol/m^{3}Pa using Equation (5) [30]. This was very similar to the Henry's constant for 35% saline water previously reported by Weiss [31].

The concentration distributions in the liquid interface where Henry's law was applied and in the liquid bulk were calculated by solving the diffusion equation using Fick's diffusion law:

$$D_{liquid}\left[\frac{\partial^2 C}{\partial x^2}\right] = \frac{\partial C}{\partial t}. \quad (6)$$

$$D_{CO_2-H_2O} = 7.4 \times 10^{-8}\left(\varnothing M_{H_2O}\right)^{1/2} T/\left(\eta_{H_2O} V^{0.6}{}_{CO_2}\right). \quad (7)$$

The Wilke–Chang equation (Equation (7)) is widely used for diffusion coefficients in liquid-phase diluted solutions. It is based on Eyring theory and the Stokes–Einstein equation. The effect of the solute is expressed by the molar volume and that of the solvent based on the molecular weight. Here, $\varnothing$ is a compounding factor that represents the effect of the combination of solvent molecules on the diffusion of the solute. This value is 2.6 when the solvent is water. M_{H_2O} is the molecular weight of water, T is the temperature, η_{H_2O} is the viscosity of water, and V_{CO_2} is the molar volume of CO_2 at an abnormal boiling point [32].

Several experimental methods have been proposed for measuring gas diffusion in liquids. The existing methods are classified into direct and indirect methods. In the conventional direct methods, the composition of the liquid phase is analyzed by sampling at various times during the experiment. The direct methods include the Taylor–Aris dispersion method proposed by Frank et al. [33], the capillary cell method used by Witherspoon and Saraf [34], and gas adsorption in a jet presented by Tang and Himmelblau [35]. The main limitations of these direct analysis methods are high pressure and temperature conditions and difficulties with sampling [33–36]. The diffusion coefficient for the experimental conditions of this study is presented in the next section.

A mathematical model for explaining the phenomenon that occurs in the seawater–CO_2 system was developed. The basic assumptions for CO_2 capture are as follows:

1. Heat transfer by conduction and radiation can be ignored in the axial direction;
2. Henry's law is applicable to the CO_2 solubility in the liquid phase;
3. Absorption reactions occur only in liquids;
4. Vaporization of liquids does not occur;
5. The reactor is adiabatic.

The boundary condition equations of diffusion are as follows:

$$\text{at } x = 0,\ C_0 = \frac{P}{H}, \quad (8)$$

$$\text{at } x = \text{L},\ \frac{\partial C}{\partial x} = 0 \text{ (insulation boundary)}. \quad (9)$$

3.3. Sensitivity Analysis

To determine mesh size, a sensitivity study was performed by reducing the mesh size by 50%. Regarding the mesh size of the model, six cases were assumed and Reactor P was calculated. The results showed that the pressure was reduced below 2% when the mesh size was smaller than 0.00024 (m), as shown in Table 3. The mesh size for analysis to determine the diffusion coefficient was determined to 0.00012 (m).

Table 3. Sensitivity scenarios.

Scenario	Mesh Size (m)	Reactor P (bar)	Sensitivity (%)
Case 1	0.00384	4.373	24.25
Case 2	0.00192	4.369	15.98
Case 3	0.00096	4.366	6.75
Case 4	0.00048	4.364	4.39
Case 5	0.00024	4.363	1.99
Case 6	0.00012	4.362	-

4. Results and Discussion

The results of the dissolution experiment and numerical analysis for distilled water and seawater at 25 and 32 °C, respectively, are presented in the following sections to verify the reliability and reproducibility of the fabricated experimental setup as well as to elucidate the long-term diffusion coefficient.

4.1. Long-Term Reaction Characteristics Using Distilled Water

Figure 2 shows the CO_2 concentration in distilled water over time according to the temperature at the equilibrium pressure of 5 bar. These experimental results were compared to the results of a simulation in which the diffusion coefficient values in Table 4 were used. The CO_2 concentration increased with the equilibrium pressure and the decrease in reactor temperature, but the dissolution velocity was dependent on the temperature according to Equation (7).

Table 4. CO_2 diffusion coefficients in water as per the literature.

Source	Method	Solution	Temperature (°C)	Diffusion Coefficient (10^{-5} cm^2/s)
Tang and Himmelblau [35]	Jet	Water	25	1.92
Unver and Himmelblau [37]	Jet	Water	6.5–65	1.145–4.296
Thomas and Adams [38]	Jet	Water	18.5–75.1	1.65–5.40
Tamimi et al. [39]	-	Water	20–80	1.76–8.20

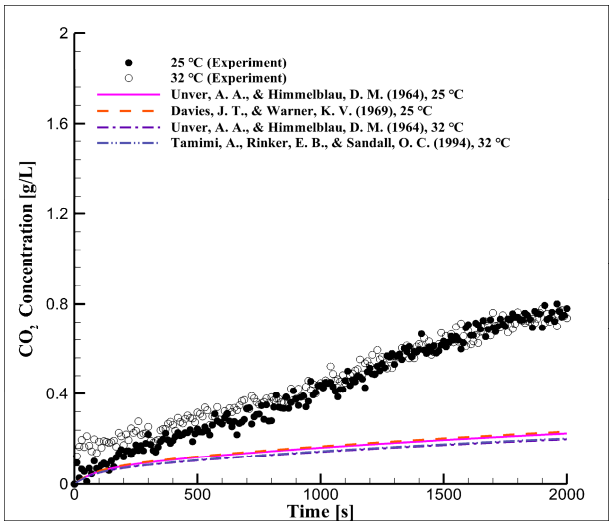
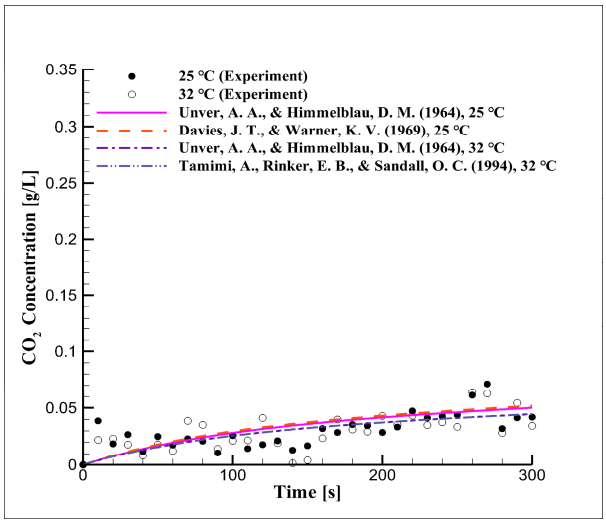


Figure 2. Long-term CO_2 concentration over time due to equilibrium pressure and temperature in distilled water.

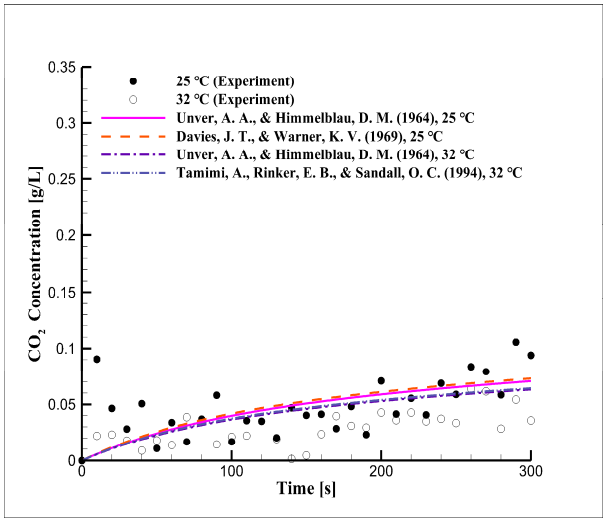
Hirai et al. [8] mentioned that the dissolution velocity increases with reaction temperature, but the difference is difficult to detect, as shown in Figure 2. The data obtained from the numerical analysis conducted using the diffusion coefficient values from the literature agree with the experimental data measured in this study at the beginning of the experiments. This agreement, however, decreased over time, which indicates that the conditions of the diffusion coefficient used for CO_2 diffusion and dissolution were different.

4.2. Short-Term Reaction Characteristics Using Distilled Water

Figure 3 shows the CO_2 concentration in distilled water over time according to the equilibrium pressure and temperature. Figure 3 shows that the diffusion and dissolution velocity of CO_2 were related to temperature. The observed concentration, using the diffusion coefficient values obtained from the literature (Table 3), was compared to the experimental results. The results of the experiments were in good agreement with those of the simulation in terms of the CO_2 concentration at the beginning of the experiments, but this agreement deviated over time.

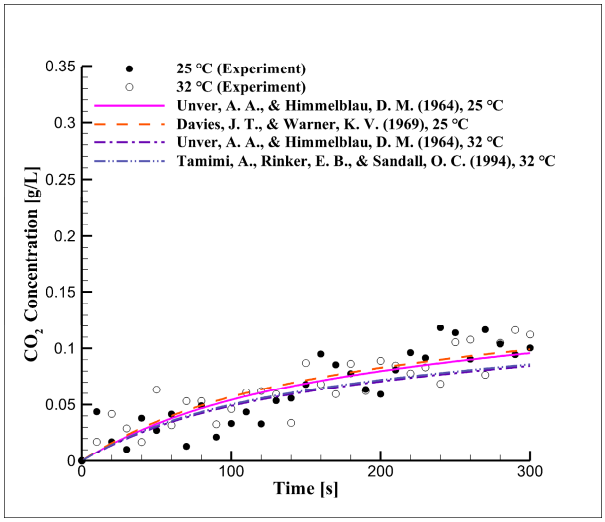


(**a**)



(**b**)

Figure 3. *Cont.*



(**c**)

Figure 3. Short-term CO_2 concentration over time due to the equilibrium pressure and temperature in distilled water at pressures of (**a**) 2, (**b**) 3, and (**c**) 5 bar.

We estimated that the CO_2 concentration would continue to increase over time according to Henry's constant. This observation showed that the diffusion coefficients obtained from the literature were substantially lower than those from the experiments. Thus, the diffusion coefficients were obtained through numerical analysis.

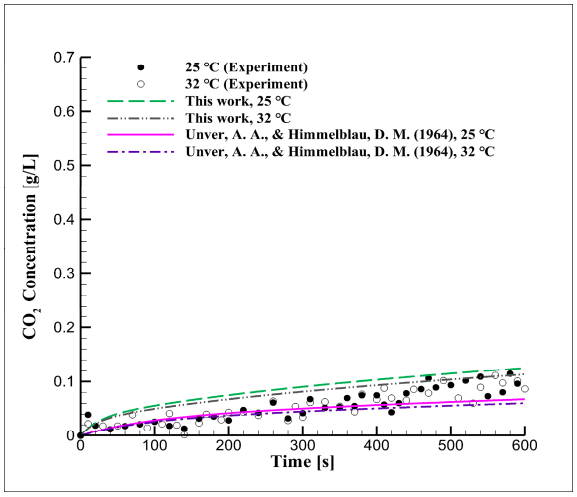
4.3. Experimental Approach Considering Concentration in Distilled Water

For the diffusion coefficient values presented in Table 4, the jet method was used as the experimental method. In this case, a very short contact time and high liquid velocity were used [40]. The diffusion coefficient values of CO_2 and water used for numerical analysis are listed in Table 4. The average standard deviation of the reported experimental values was 0.1×10^{-5} cm^2/s at 25 °C.

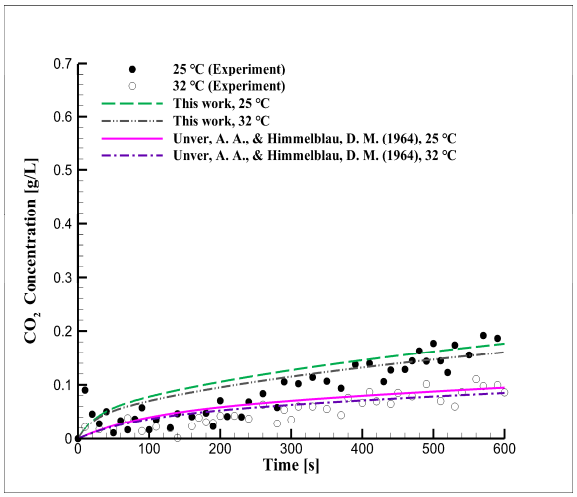
4.4. Mid-Term Reaction Characteristics Using Distilled Water

One important prerequisite for the accurate simulation of CO_2 diffusion is an appropriate CO_2–H_2O diffusion coefficient. The diffusion coefficient derived though numerical analysis was introduced and the results were compared to those obtained experimentally. The CO_2 diffusion coefficient in distilled water was 7.06×10^{-5} cm^2/s at 25 °C and 8.56×10^{-5} cm^2/s at 32 °C.

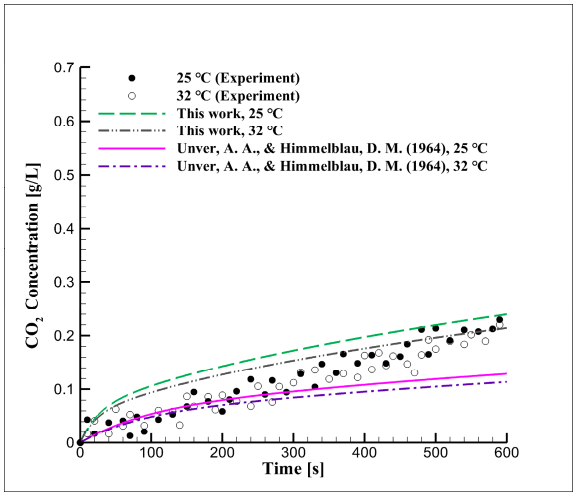
Figure 4 shows the simulation data obtained by applying the derived diffusion coefficient values and experimental data at changing equilibrium pressure and temperature. As the derived diffusion coefficient increased, the CO_2 concentration increased in the simulation results, which is in good agreement with the experimental results. According to this, the diffusion coefficient of CO_2 increases with the temperature and the diffusion coefficient increases as the contact time increases, unlike in previous studies that derived the diffusion coefficients for very short periods of time using the jet method.



(**a**)



(**b**)



(**c**)

Figure 4. Mid-term CO_2 concentration over time due to changes in the equilibrium pressure and temperature in distilled water at pressures of (**a**) 2, (**b**) 3, and (**c**) 5 bar.

4.5. Experimental Approach Considering Concentration in Seawater

This section describes the attempt to derive the concentration of CO_2 and the diffusion coefficient according at equilibrium pressure and experimental temperatures under seawater conditions by increasing the salinity.

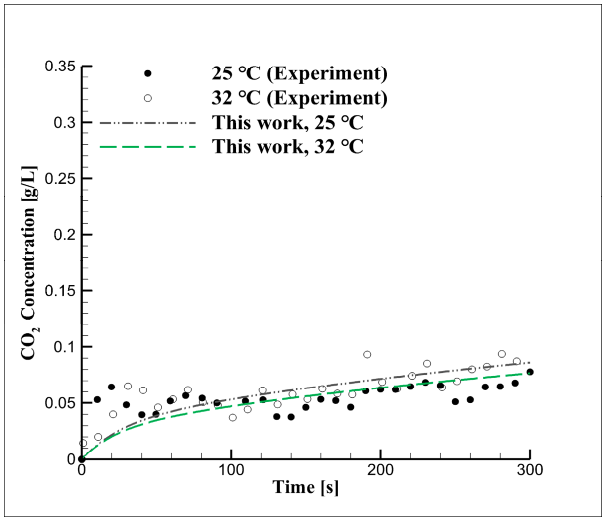
Table 5 summarizes the CO_2 diffusions coefficient in brine provided in the literature. As shown, most of the studies on the CO_2 diffusion coefficient in seawater were conducted under high-pressure, high-temperature, and supercritical conditions and the diffusion coefficient was derived under extreme conditions. As studies on CO_2 absorption capacity of seawater at normal temperature and pressure are not sufficient, estimating the seawater–CO_2 diffusion coefficient under ordinary conditions was attempted through experiments and simulations.

Table 5. CO_2 diffusion coefficients in brine as found in the literature.

Source	Solution	Pressure (kPa)	Temperature (°C)	Diffusion Coefficient (10^{-5} cm^2/s)
Renner [41]	Brine	2186–5861	25	9.07–9.86
Wang et al. [42]	Brine	1524–5178	38	2.93–4.83
Yang C and Gu [43]	Brine	2600–7500	27–58	170.7–269.8
Azin et al. [44]	Brine	5858–6898	40–45	3.52–6.16
Mojtaba et al. [45]	Brine	3450	38	1.75
Zhang et al. [46]	Brine	1170	25	1.5–1.91

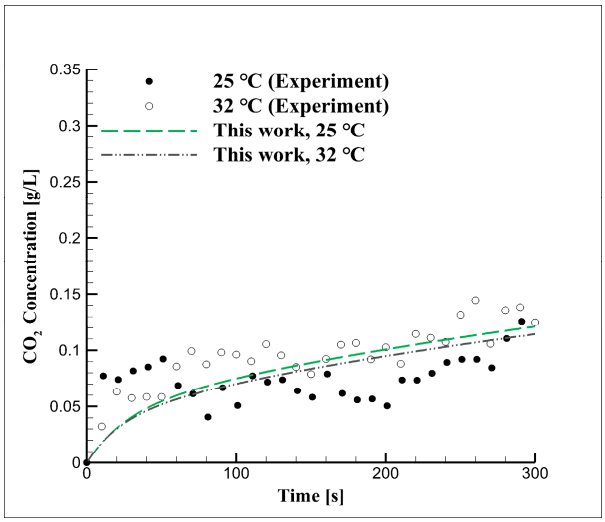
4.6. Short-Term Reaction Characteristics in Seawater

Figure 5 shows the CO_2 concentration in seawater over time based on the results of the six diffusion experiments performed under the equilibrium pressures of 2, 3, and 5 bar and the temperatures of 25 and 32 °C. The concentration of CO_2 increased with the increase in equilibrium pressure and the decrease in reaction temperature, while the dissolution velocity of CO_2 was determined using Equation (7). As shown in Table 5, previous studies derived the CO_2 diffusion coefficient under high-pressure and high-temperature conditions. In Figure 5, the seawater–CO_2 diffusion coefficient for the corresponding conditions is shown based on the simulation using numerical modeling.

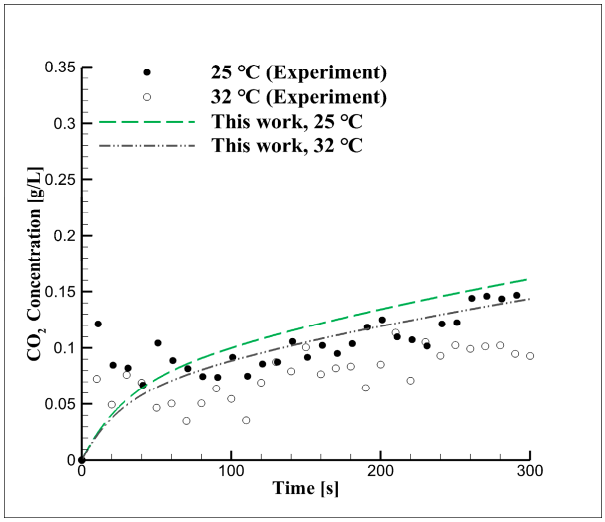


(**a**)

Figure 5. *Cont.*



(**b**)



(**c**)

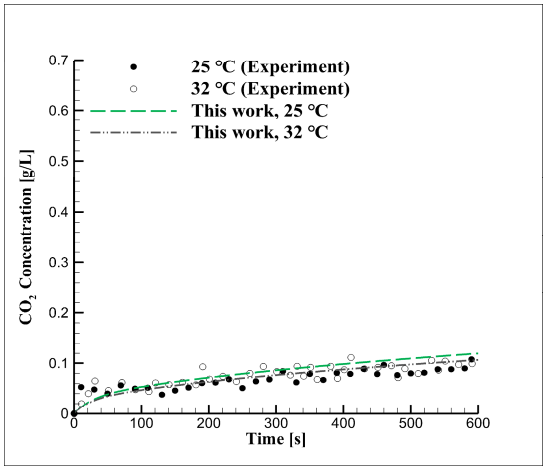
Figure 5. Short-term CO_2 concentration over time due to changes in equilibrium pressure and temperature in seawater at pressures of (**a**) 2, (**b**) 3, and (**c**) 5 bar.

The CO_2 concentration increased with the equilibrium pressure and it decreased or increased as the temperature increased. The CO_2 diffusion coefficient in seawater estimated through the simulation was 6.3×10^{-5} cm^2/s at 25 °C and 7.24×10^{-5} cm^2/s at 32 °C.

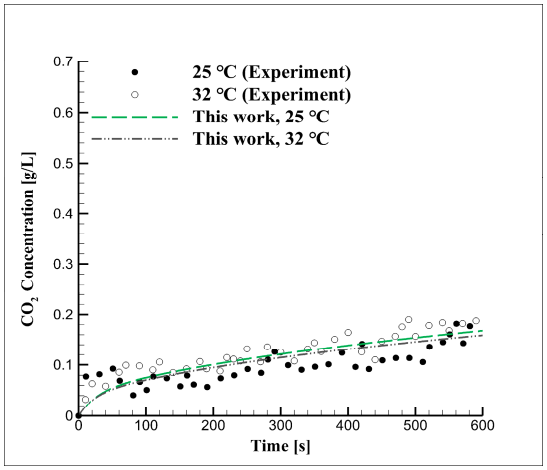
4.7. Mid-Term Reaction Characteristics in Seawater

Figure 6 shows the concentration of CO_2 in seawater over time, up to 600 s under equilibrium pressures of 2, 3, and 5 bar and temperatures of 25 and 32 °C. When the numerical analysis was conducted by applying the diffusion coefficient values selected from Figure 5, the concentration of CO_2 increased with the increase in equilibrium pressure, which is in good agreement with the experimental results. The diffusion coefficient in seawater was approximately 17% lower than that in distilled water. Many ions and types of organic matter exist in seawater and the CO_2 diffusion coefficient decreased as the total dissolved solids increased. Moreover, the concentration of CO_2 in seawater decreased with the increase in salinity and the diffusion coefficient in seawater was low because of limited CO_2

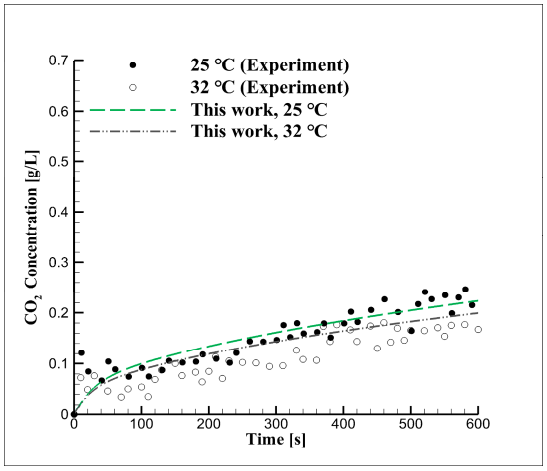
diffusion. When CO_2 is dissolved in water, it is divided into $D_{HCO_3^-}$ and $D_{CO_3^{2-}}$. These components have different diffusion coefficients whose effects become visible over time [46,47].



(**a**)



(**b**)



(**c**)

Figure 6. Mid-term CO_2 concentration over time due to changes in equilibrium pressure and temperature in seawater at pressures of (**a**) 2, (**b**) 3, and (**c**) 5 bar.

Table 6 lists shows the optimized CO_2 diffusion coefficient results obtained when distilled water and seawater were used as solvents at normal pressure and temperature. The diffusion coefficient values estimated experimentally were approximately three-times higher than the reference diffusion coefficient values in distilled water. Following previous studies [34,37,39], the CO_2 diffusion coefficient was presented using the jet method. As the contact time between the liquid and gas is very short and the liquid velocity is high in the jet method, differences from the D values estimated from the experiments are observable at long experimental times. The reference diffusion coefficient values in seawater were based on the high-pressure, high-temperature, and supercritical conditions (Table 5), which were not consistent with the experimental conditions. The CO_2 diffusion coefficient in seawater obtained through the numerical analysis under the experimental conditions was 6.3×10^{-5} cm^2/s at 25 °C and 7.24×10^{-5} cm^2/s at 32 °C. The CO_2 diffusion coefficient at 32 °C was approximately 13% higher than that at 25 °C.

Table 6. Comparison of CO_2 diffusion coefficients by temperature.

	Diffusion Coefficient (10^{-5} cm^2/s)			
	Distilled Water		**Seawater**	
	25 °C	32 °C	25 °C	32 °C
Reference	1.85–2.0	2.08–2.16	-	-
Experiment	7.06	8.56	6.3	7.24

5. Conclusions

This study was conducted to investigate the characteristics of the CO_2 diffusion coefficient, an essential element that affects the concentration of CO_2 over time, in the treatment of the residual gas generated in a vessel by dissolving it in seawater and discharging it to the outside of the vessel. The temperature and solvent, which affect the CO_2 diffusion coefficient, were examined by using a theoretical approach, conducting dissolution experiments, and analyzing the dynamic characteristics. The following conclusions were drawn:

(1) For the treatment of the residual gas generated in the reformer, the concentration of CO_2, a residual gas component, was observed at different pressures and temperatures from the perspective of dissolution using seawater and the CO_2 diffusion coefficient was derived through numerical analysis using MATLAB;

(2) It was confirmed that the experimental time, temperature, and pressure could be variables in selecting the CO_2 diffusion coefficient for each solvent;

(3) The CO_2 concentration in seawater was approximately 55% higher when the equilibrium pressure was 5 bar and the reaction temperature was 25 °C than when these parameters were 2 bar and 32 °C;

(4) Under the actual operating conditions of underwater weapon systems, the CO_2 diffusion coefficient in distilled water and seawater, according to the dissolution time, was derived by temperature. The CO_2 diffusion coefficient in seawater was 6.3×10^{-5} cm^2/s at 25 °C and 7.24×10^{-5} cm^2/s at 32 °C. The CO_2 diffusion coefficient was approximately 13% higher at 32 °C than at 25 °C;

(5) It is possible to accurately estimate the concentration of CO_2, a residual gas component of the reformer, under the operating conditions of each vessel using the derived CO_2 diffusion coefficient as a function of temperature.

If a process for estimating the concentration of the residual gas generated in a reformer is implemented using the seawater–CO_2 diffusion coefficient based on the results from the actual operating conditions of underwater weapon systems, innovative developments will be possible.

Author Contributions: Supervision, J.C.; Methodology, J.C. and E.-Y.P.; Investigation, J.C. and E.-Y.P.; Funding acquisition, J.C.; Writing—review and editing, J.C. and E.-Y.P. All authors have read and agreed to the published version of the manuscript.

Funding: This work was supported by the Dong-A University Research Fund.

Acknowledgments: This research was supported by the Agency for Defense Development funded by the Defense Acquisition Program Administration [Project Name: 17-113-407-039].

Conflicts of Interest: The authors declare no conflict of interest.

References

1. Psoma, A.; Sattler, G. Fuel cell systems for submarines: from the first idea to serial production. *J. Power Sources* **2002**, *106*, 381–383. [CrossRef]
2. Brighton, D.R.; Mart, P.L.; Clark, G.A.; Rowan, M.J.M. The use of fuel cells to enhance the underwater performance of conventional diesel electric submarines. *J. Power Sources* **1994**, *51*, 375–389. [CrossRef]
3. Rostami, H.; Zhiani, M.; Zamani, A.R.; Madhkhan, M. Fuel cells application in subsea industries. In Proceedings of the 3rd Fuel Cell Seminar of Iran, Tehran, Iran, 28 October 2009.
4. Krummrich, S.; Llabrés, J. Methanol reformer–The next milestone for fuel cell powered submarines. *Int. J. Hydrog. Energ.* **2015**, *40*, 5482–5486. [CrossRef]
5. Cavenati, S.; Grande, C.A.; Rodrigues, A.E. Adsorption equilibrium of methane, carbon dioxide, and nitrogen on zeolite 13X at high pressures. *J. Chem. Eng. Data* **2004**, *49*, 1095–1101. [CrossRef]
6. Dash, S.K.; Samanta, A.N.; Bandyopadhyay, S.S. Experimental and theoretical investigation of solubility of carbon dioxide in concentrated aqueous solution of 2-amino-2-methyl-1-propanol and piperazine. *J. Chem. Thermodyn.* **2012**, *51*, 120–125. [CrossRef]
7. Manic, M.S.; Queimada, A.J.; Macedo, E.A.; Najdanovic-Visak, V. High-pressure solubilities of carbon dioxide in ionic liquids based on bis (trifluoromethylsulfonyl) imide and chloride. *J. Supercrit. Fluid.* **2012**, *65*, 1–10. [CrossRef]
8. Hirai, S.; Okazaki, K.; Araki, N.; Yazawa, H.; Ito, H.; Hijikata, K. Transport phenomena of liquid CO_2 in pressurized water flow with clathrate-hydrate at the interface. *Energ. Conserv. Manag.* **1996**, *37*, 1073–1078. [CrossRef]
9. Dang, H.; Rochelle, G.T. CO_2 absorption rate and solubility in monoethanolamine/piperazine/water. *Sep. Sci. Technol.* **2003**, *38*, 337–357. [CrossRef]
10. Faiz, R.; Al-Marzouqi, M. CO_2 removal from natural gas at high pressure using membrane contactors: model validation and membrane parametric studies. *J. Membr. Sci.* **2010**, *365*, 232–241. [CrossRef]
11. Lawal, A.; Wang, M.; Stephenson, P.; Yeung, H. Dynamic modelling of CO_2 absorption for post combustion capture in coal-fired power plants. *Fuel* **2009**, *88*, 2455–2462. [CrossRef]
12. Munusamy, K.; Sethia, G.; Patil, D.V.; Rallapalli, P.B.S.; Somani, R.S.; Bajaj, H.C. Sorption of carbon dioxide, methane, nitrogen and carbon monoxide on MIL-101 (Cr): Volumetric measurements and dynamic adsorption studies. *Chem. Eng. J.* **2012**, *195*, 359–368. [CrossRef]
13. Breault, R.W.; Huckaby, E.D. Parametric behavior of a CO_2 capture process: CFD simulation of solid-sorbent CO_2 absorption in a riser reactor. *Appl. Energy* **2013**, *112*, 224–234. [CrossRef]
14. Zhang, Z.; Yan, Y.; Zhang, L.; Chen, Y.; Ju, S. CFD investigation of CO_2 capture by methyldiethanolamine and 2-(1-piperazinyl)-ethylamine in membranes: Part B. Effect of membrane properties. *J. Nat. Gas Sci. Eng.* **2014**, *19*, 311–316. [CrossRef]
15. Giammanco, C.H.; Kramer, P.L.; Yamada, S.A.; Nishida, J.; Tamimi, A.; Fayer, M.D. Carbon dioxide in an ionic liquid: Structural and rotational dynamics. *J. Chem. Phys.* **2016**, *144*, 104506. [CrossRef] [PubMed]
16. Kim, J.; Pham, D.A.; Lim, Y.I. Gas–liquid multiphase computational fluid dynamics (CFD) of amine absorption column with structured-packing for CO_2 capture. *Comput. Chem. Eng.* **2016**, *88*, 39–49. [CrossRef]
17. *Standard Practice for the Preparation of Substitute Ocean Water (ASTM D1141-98)*; ASTM International: West Conshohocken, PA, USA, 1998.
18. Liu, S.; Kvamme, B. Improved Newton Raphson Method–An Effective Tool in Solving Flow-Mechanic-Chemistry Equations of CO_2 Storage in Saline Aquifers. In Proceedings of the American Conference on Applied Mathematics (MATH 08), Harvard, MA, USA, 24–26 March 2008.

19. Jiang, N.; Deng, Z.; Liu, S.; Tang, C.; Wang, G. Synthesis of metal organic framework (MOF-5) with high selectivity for CO_2/N_2 separation in flue gas by maximum water concentration approach. *Korean J. Chem. Eng.* **2016**, *33*, 2747–2755. [CrossRef]
20. Chen, Y.; Gao, Y.; Zhao, Y.; Chen, L.; Dong, C.; Sun, B. Experimental investigation of different factors influencing the replacement efficiency of CO_2 for methane hydrate. *Appl. Energy* **2018**, *228*, 309–316. [CrossRef]
21. Westerwalbesloh, C.; Grünberger, A.; Stute, B.; Weber, S.; Wiechert, W.; Kohlheyer, D.; von Lieres, E. Modeling and CFD simulation of nutrient distribution in picoliter bioreactors for bacterial growth studies on single-cell level. *Lab Chip* **2015**, *15*, 4177–4186. [CrossRef]
22. Luo, Y.; Yang, H.; Lu, L.; Qi, R. A review of the mathematical models for predicting the heat and mass transfer process in the liquid desiccant dehumidifier. *Renew. Sustain. Energy Rev.* **2014**, *31*, 587–599. [CrossRef]
23. Wang, C.; Xu, Z.; Lai, C.; Sun, X. Beyond the standard two-film theory: Computational fluid dynamics simulations for carbon dioxide capture in a wetted wall column. *Chem. Eng. Sci.* **2018**, *184*, 103–110. [CrossRef]
24. Liu, Y.; Pan, J.; Tang, A.; Wang, Q. A study on mass transfer–reaction kinetics of NO absorption by using UV/H_2O_2/NaOH process. *Fuel* **2013**, *108*, 254–260. [CrossRef]
25. Kashid, M.N.; Renken, A.; Kiwi-Minsker, L. Gas–liquid and liquid–liquid mass transfer in microstructured reactors. *Chem. Eng. Sci.* **2011**, *66*, 3876–3897. [CrossRef]
26. Fu, K.; Chen, G.; Sema, T.; Zhang, X.; Liang, Z.Z.; Idem, R.; Tontiwachwuthikul, P. Experimental study on mass transfer and prediction using artificial neural network for CO_2 absorption into aqueous DETA. *Chem. Eng. Sci.* **2013**, *100*, 195–202. [CrossRef]
27. Ma, S.; Chen, G.; Zhu, S.; Han, T.; Yu, W. Mass transfer of ammonia escape and CO_2 absorption in CO_2 capture using ammonia solution in bubbling reactor. *Appl. Eng.* **2016**, *162*, 354–362. [CrossRef]
28. Sander, R. Compilation of Henry's law constants (version 4.0) for water as solvent. *Atmos. Chem. Phys.* **2015**, *15*, 4399–4981. [CrossRef]
29. Harvey, A.H.; Smith, F.L. Avoid common pitfalls when using Henry's law. *Chem. Eng. Prog.* **2007**, *103*, 33–39.
30. Dalmolin, I. Solubility of carbon dioxide in binary and ternary mixtures with ethanol and water. *Fluid Phase Equilibria* **2006**, *245*, 193–200. [CrossRef]
31. Weiss, R.F. Carbon dioxide in water and seawater: the solubility of a non-ideal gas. *Mar. Chem.* **1974**, *2*, 203–215. [CrossRef]
32. Hirai, S.; Okazaki, K.; Yazawa, H.; Ito, H.; Tabe, Y.; Hijikata, K. Measurement of CO_2 diffusion coefficient and application of LIF in pressurized water. *Energy* **1997**, *22*, 363–367. [CrossRef]
33. Frank, M.J.W.; Kuipers, J.A.M.; van Swaaij, W.P. Diffusion coefficients and viscosities of CO_2 + H_2O, CO_2 + CH_3OH, NH_3 + H_2O, and NH^{3+} CH_3OH liquid mixtures. *J. Chem. Eng. Data* **1996**, *41*, 297–302. [CrossRef]
34. Witherspoon, P.A.; Saraf, D.N. Diffusion of methane, ethane, propane, and n-butane in water from 25 to 43. *J. Phys. Chem.* **1965**, *69*, 3752–3755. [CrossRef]
35. Tang, Y.P.; Himmelblau, D.M. Effect of solute concentration on the diffusivity of carbon dioxide in water. *Chem. Eng. Sci.* **1965**, *20*, 7–14. [CrossRef]
36. Shi, Z.; Wen, B.; Hesse, M.A.; Tsotsis, T.T.; Jessen, K. Measurement and modeling of CO_2 mass transfer in brine at reservoir conditions. *Adv. Water Res.* **2018**, *113*, 100–111. [CrossRef]
37. Unver, A.A.; Himmelblau, D.M. Diffusion coefficients of CO_2, C_2H_4, C_3H_6 and C_4H_8 in water from 6 to 65 C. *J. Chem. Eng. Data* **1964**, *9*, 428–431. [CrossRef]
38. Thomas, W.J.; Adams, M.J. Measurement of the diffusion coefficients of carbon dioxide and nitrous oxide in water and aqueous solutions of glycerol. *Trans. Faraday Soc.* **1965**, *61*, 668–673. [CrossRef]
39. Tamimi, A.; Rinker, E.B.; Sandall, O.C. Diffusion coefficients for hydrogen sulfide, carbon dioxide, and nitrous oxide in water over the temperature range 293-368 K. *J. Chem. Eng. Data* **1994**, *39*, 330–332. [CrossRef]
40. Nijsing, R.A.T.O.; Hendriksz, R.H.; Kramers, H. Absorption of CO_2 in jets and falling films of electrolyte solutions, with and without chemical reaction. *Chem. Eng. Sci.* **1959**, *10*, 88–104. [CrossRef]
41. Renner, T.A. Measurement and correlation of diffusion coefficients for CO_2 and rich-gas applications. *SPE Reserv. Eng.* **1988**, *3*, 517–523. [CrossRef]
42. Wang, L.-S.; Lang, Z.-X.; Guo, T.-M. Measurement and correlation of the diffusion coefficients of carbon dioxide in liquid hydrocarbons under elevated pressures. *Fluid Phase Equilibria* **1996**, *117*, 364–372. [CrossRef]

43. Yang, C.; Gu, Y. Accelerated mass transfer of CO_2 in reservoir brine due to density-driven natural convection at high pressures and elevated temperatures. *Ind. Eng. Chem. Res.* **2006**, *45*, 2430–2436. [CrossRef]
44. Azin, R.; Mahmoudy, M.; Raad, S.M.J.; Osfouri, S. Measurement and modeling of CO_2 diffusion coefficient in saline aquifer at reservoir conditions. *Cent. Eur. J. Eng.* **2013**, *3*, 585–594. [CrossRef]
45. Mojtaba, S.; Behzad, R.; Rasoul, N.M.; Mohammad, R. Experimental study of density-driven convection effects on CO_2 dissolution rate in formation water for geological storage. *J. Nat. Gas Sci. Eng.* **2014**, *21*, 600–607. [CrossRef]
46. Zhang, W.; Wu, S.; Ren, S.; Zhang, L.; Li, J. The modeling and experimental studies on the diffusion coefficient of CO_2 in saline water. *J. CO_2 Util.* **2015**, *11*, 49–53. [CrossRef]
47. Zeebe, R.E. On the molecular diffusion coefficients of dissolved CO_2, HCO_3^-, and CO_3^{2-} and their dependence on isotopic mass. *Geochim. Cosmochim. Acta* **2001**, *75*, 2483–2498. [CrossRef]



© 2020 by the authors. Licensee MDPI, Basel, Switzerland. This article is an open access article distributed under the terms and conditions of the Creative Commons Attribution (CC BY) license (http://creativecommons.org/licenses/by/4.0/).